Modes and rates of horizontal deformation from rotated river basins: Application to the Dead Sea fault system in Lebanon

Liran Goren[1], Sébastien Castelltort[2], and Yann Klinger[3]
[1]Geological and Environmental Sciences, Ben-Gurion University of the Negev, Beer Sheva, 84105, Israel
[2]Section des Sciences de la Terre et de l'Environnement, Université de Genève, Rue des Maraîchers 13, 1205 Geneva, Switzerland
[3]Institut de Physique du Globe de Paris, Sorbonne Paris Cité, Université Paris Diderot, UMR7154 CNRS, 75238 Paris, France

ABSTRACT

Partitioning of horizontal deformation between localized and distributed modes in regions of oblique tectonic convergence is, in many cases, hard to quantify. Here we use the geometry of river basins and numerical modeling to evaluate modes and rates of horizontal deformation associated with the Arabia-Sinai relative plate motion in Lebanon. We focus on river basins that drain Mount Lebanon to the west and are bounded by the Yammouneh fault, a segment of the Dead Sea fault system that transfers left-lateral deformation across the Lebanese restraining bend. We quantify a systematic counterclockwise rotation of these basins and evaluate drainage area disequilibrium using the χ metric. The analysis indicates a systematic spatial pattern whereby tributaries of the rotated basins appear to experience drainage area loss or gain with respect to channel length. A kinematic model reveals that since the late Miocene, 23%–31% of the relative plate motion parallel to the plate boundary has been distributed along a wide band of deformation to the west of the Yammouneh fault. Taken together with previous, shorter-term estimates, the model indicates little variation of slip rate along the Yammouneh fault since the late Miocene. Kinematic model results are compatible with late Miocene paleomagnetic rotations in western Mount Lebanon. A numerical landscape evolution experiment demonstrates the emergence of a similar pattern of drainage area disequilibrium in response to progressive distributed shear deformation of river basins with relatively minor drainage network reorganization.

INTRODUCTION

Theory (e.g., Sanderson and Marchini, 1984; Teyssier et al., 1995) and observations (e.g., Vallage et al., 2014) of regions of oblique tectonic convergence have demonstrated that deformation in such settings is commonly partitioned into localized (faults) and distributed zones of pure or combined convergence and shear in variable ratios. In such situations, knowledge of long-term relative plate velocity is insufficient for estimating geological slip rates on the main faults, which hinders our understanding of the related regional tectonics.

Rivers are commonly used as offset markers across strike-slip faults (e.g., Klinger et al., 2000), and entire river basins have been suggested to record large-scale distributed horizontal deformation (Hallet and Molnar, 2001; Ramsey et al., 2007; Castelltort et al., 2012). Here we use morphometric analysis of river basins and modeling to constrain rates and modes of localized and distributed deformation along the Lebanese segment of the Dead Sea fault system (DSFS).

THE DEAD SEA FAULT SYSTEM IN LEBANON

The DSFS accommodates the left-lateral motion between Sinai and Arabia plates (Freund et al., 1970). Along Lebanon, the DSFS bends 30°E, forming a 180-km-long restraining bend (Fig. 1). The left-lateral Yammouneh fault (YF) and the Serghaya fault are the two main structures that run along the sides of Bekaa Valley (Fig. 1).

By contrast, the Beirut-Tripoli thrust system off-shore of Lebanon accommodates mainly dip-slip motion (Elias et al., 2007; Carton et al., 2009).

The YF, the sole continuous structure across the Lebanese bend, has been suggested to accommodate the fastest slip in the area (Daëron et al., 2004). However, there are gaps and uncertainties in our understanding of the kinematic history of the Arabia-Sinai plate boundary along the Lebanese restraining bend. For example, how much of the relative plate velocity is taken up by the YF is still debated. This is partly reflected in the relatively wide range of slip rates, 3.8–6.4 mm/yr, that have been proposed for the YF (Daëron et al., 2004; Gomez et al., 2006, 2007). Furthermore, these rates are considered relevant for Holocene/Quaternary times, but the onset of relative motion has been suggested to date back to the late Miocene (Quennell, 1984; Ben-Avraham et al., 2008).

Moreover, paleomagnetic measurements of ~30° counterclockwise rotation along an ~30-km-wide region west of the YF (Van Dongen et al., 1967; Gregor et al., 1974; Ron, 1987; Henry et al., 2010) suggest distributed deformation off the major faults (McKenzie and Jackson, 1983). However, the timing of the rotation and its relation to the DSFS activity remain poorly constrained (Gomez et al., 2007).

ROTATED RIVERS

We determine the orientation of river basins in western Mount Lebanon (Fig. 1) by orthogo-
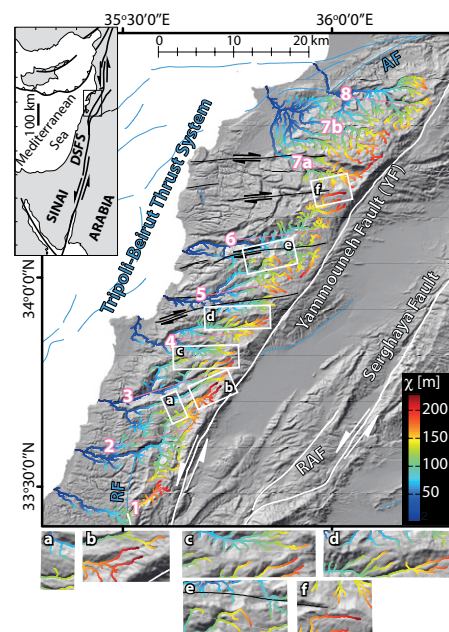

Figure 1. Shaded relief map of study area along the Lebanese restraining bend. White thick lines are sinistral strike-slip faults, blue lines are thrust faults, and black lines are oblique dextral strike-slip normal faults. DSFS—Dead Sea fault system; RAF—Rachaya fault; RF—Roum fault; AF—Akkar fault. Drainage network of western Mount Lebanon is colored by χ (see Equation 1) with $m/n = 0.3$ and $A_0 = 1$ km² (m/n is the concavity index, A_0 is an arbitrary scaling area; see the Data Repository [see footnote 1]). Pink lines show basin orientation calculated by using weighted orthogonal linear regression (see the Data Repository). Enlargements of boxes a–f show χ differences across divides.

nal linear regression through the pixels of each basin, weighted by upstream drainage area (see the GSA Data Repository[1]). River basins 2–6 (Fig. 1) show a systematic pattern of 41° ± 3° counterclockwise rotation with respect to the typical transverse drainage orientation of linear mountain ranges (Hovius, 1996) such as Mount Lebanon. We suggest that these five rivers be-

have as markers of the time-integrated velocity field to the west of the YF and thus indicate significant distributed horizontal crustal deformation in the area (e.g., Castelltort et al., 2012).

At both ends of the restraining bend, river basins show a different pattern and are ignored in our analysis. In the north, basins 7 and 8 could have been affected by the change of orientation of the YF (Fig. 1, inset) and interacted with the Akkar fault (Elias et al., 2007), which could have led to significant drainage reorganization. In the south, basin 1 is offset by the Roum fault (Fig. 1), and its orientation reflects both distributed and localized deformation.

DRAINAGE AREA DISEQUILIBRIUM

Our hypothesis is that basins 2–6 and their river networks are advected and deformed together with the crust over which they are imprinted. Therefore, the drainage network topology and the distribution of stream length and drainage area in these basins are transient features and are expected to be in a state of disequilibrium. We investigate this transiency by using the χ metric (Perron and Royden, 2013), which is defined along fluvial channels as:

$$\chi(x) = \int_0^x \left(\frac{A_0}{A(x')} \right)^{\frac{m}{n}} dx', \quad (1)$$

where A is the upstream drainage area, A_0 is an arbitrary scaling area, x is distance along channel, x' is the variable of integration, and m and n are positive empirical constants. The integral in Equation 1 is taken from the base level ($x = 0$) to a position x along a channel. Under a common pattern and history of rock uplift rate, U, and of erosivity, K, that reflects runoff characteristics and rock erodibility, there is a one-to-one mapping between the expected elevation at steady state and the value of χ (Perron and Royden, 2013).

Therefore, when χ is mapped along a fluvial channel system and shows different values between two adjacent channel heads across a water divide, the assumption of U and K commonality or the assumption of steady state is violated (Willett et al., 2014). Such χ differences can arise from variations of the tectonic history and erosivity pattern of the two channels between the divide and the channels' confluence, or they can arise from disequilibrium in the drainage area distribution such that the position of the water divide is not optimal and perhaps transient (Willett et al., 2014; Shelef and Hilley, 2014).

Figure 1 shows that within each of the central and southern basins, the value of χ is systematically higher along northern tributaries with respect to southern tributaries. Thus, χ differences arise across internal divides within each basin and across the divides that separate these basins, with high χ values to the south of each inter-basin divide and low χ to its north. This periodic pattern of χ differences can result from periodic variation of U and K along strike

with a wavelength equal to the width of a single basin, a scenario for which there is no evidence. Hence, following previous interpretations of similar χ behavior in other settings (Willett et al., 2014; Shelef and Hilley, 2014; Yang et al., 2015), we suggest that the pattern is indicative of disequilibrium in drainage area distribution and in divide position. This view is supported by the landscape morphology showing high-χ perched channels and asymmetric hillslopes that are steeper toward low-χ channels (Fig. DR5 in the Data Repository).

KINEMATIC MODEL

We develop a kinematic model of distributed deformation along a wide band between the YF and the offshore Beirut-Tripoli thrust system.

River basins 2–6 are assumed to be the end product of shearing of a drainage network that was initially perpendicular to the main axis of the range (Hovius, 1996) prior to the current episode of deformation, with headwaters of basin 6 at the northern kink of the YF. According to our hypothesis, these rivers were simultaneously deformed by southward translation and counterclockwise rotation, leading to their current orientation. The northern kink of the YF defines the origin of the coordinate system, with x-axis and y-axis perpendicular (positive westward) and parallel (positive southward) to the YF, respectively (Fig. 2). The velocity field is defined with respect to a fixed block east of the YF. The fault-parallel and fault-perpendicular velocities, V and U respectively, decrease linearly eastward from a far-field value, V_p and U_p, to a fault value, V_f and $U_f = 0$, immediately to the west of the YF (Daëron et al., 2004; Gomez et al., 2006). We can express U and V as functions of x and the width of the band of deformation, R_d (Fig. 2):
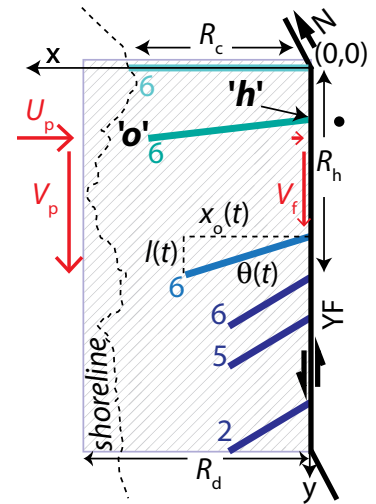
$$U(x) = -\frac{U_p}{R_d} x, \quad (2)$$

$$V(x) = -\frac{V_p - V_f}{R_d} x + V_f. \quad (3)$$

We consider a single river as a straight line that stretches westward from the YF. The velocity field prescribed by Equations 2 and 3 can be used to find the deviation angle, θ, of the line river as a function of V_f (see the Data Repository):

$$\tan\theta(V_f) = \frac{V_p - V_f}{U_p} \left[\exp\left(\frac{U_p}{R_d} \frac{R_h}{V_f} \right) - 1 \right], \quad (4)$$

where $R_h = tV_f$ is the distance of the headwaters of basin 6 from the origin (the fault kink) at time t. $R_h = 30$ km is measured on the map. To estimate V_p and U_p, the relative plate velocity from Arabia-Sinai poles of rotation of Le Pichon and Gaulier (1988) (see the Data Repository) is decomposed into a component perpendicular to the YF, 4.2 mm/yr, and a component parallel to the YF, 7.0 mm/yr. In the kinematic model, we
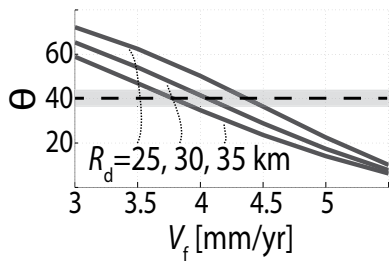

Figure 2. Plan view of kinematic model. YF—Yammouneh fault, R_h—distance of the current position of basin 6 from the origin, R_d—width of the band of deformation, R_c—width of the zone along which the distributed deformation affects the rivers. x-axis is positive to the west, and y-axis is positive to the south. Red arrows represent the velocity field along western Mount Lebanon. V_p and U_p are far-field fault-parallel and fault-perpendicular velocities, respectively. V_f is fault-parallel velocity immediately to the west of the YF. Points 'o' and 'h' mark western end and headwater of the advected line-river, respectively. $x_o(t)$ is x coordinate of point 'o' at time t, $l(t)$ is y-axis projection of the line-river at time t, and $\theta(t)$ is deviation angle of the line-river from a fault-perpendicular orientation at time t. Line-river color becomes darker as it progressively translates to the south and rotates counterclockwise. Numbers refer the basins in Figure 1.

choose $U_p = 4.2$ mm/yr (such that all the convergence is accommodated to the west of the YF). We account for an average, post–mid-Miocene, slip rate of 1 mm/yr along the Serghaya fault (Gomez et al., 2006), which leaves $V_p = 6.0$ mm/yr. R_d, the width of the band of deformation, is unknown, but we estimate that it varies between 25 km, the distance from the YF to the western end of the Lebanese flexure, to 35 km, the distance from the YF to the proximal parts of the Beirut-Tripoli thrust system.

Figure 3 shows θ as a function of V_f computed with Equation 4 for three values of R_d. The gray bar represents the range of orientations of basins 2–6 and thus indicates that V_f ranges between 3.8 and 4.4 mm/yr. As a consequence, given $t = R_h/V_f$, the duration of the episode of distributed deformation that has led to the current configuration is in the range $t = 6.8$–7.9 m.y. for $R_d = 25$–35 km.

LANDSCAPE EVOLUTION MODELING

We use a numerical model of landscape evolution (Goren et al., 2014) to test the hypothesis that river orientation and the anomalous χ pat-

Figure 3: Results of kinematic model showing river deviation angle, θ, as function of average slip rate on Yammouneh fault, V_f. Three gray curves are solution of Equation 4 for three values of R_d (width of band of deformation), from bottom to top R_d = 35, 30, and 25 km. Light gray bar and dashed line show range and average deviation, respectively, of basins 2–6 (Fig. 1).
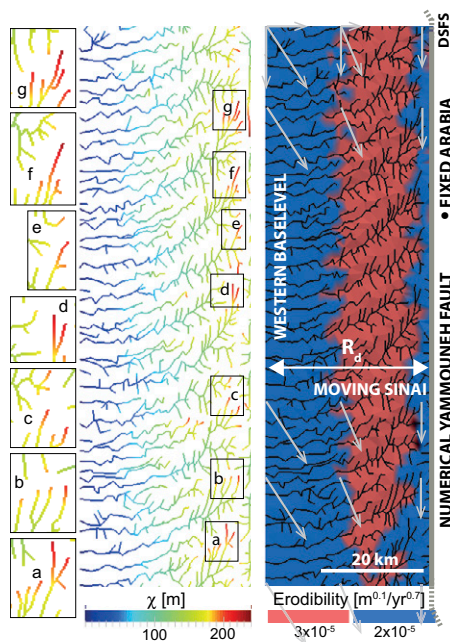
tern both result from the proposed distributed deformation. The numerical model adds a degree of freedom with respect to the kinematic model, as here rivers can oppose deformation by reorganization of the drainage network. The numerical domain of a linear mountain range starts from a subdued topography (Gomez et al., 2006). We then simultaneously impose a sudden increase in uplift rate (see the Data Repository) and a horizontal velocity field between the western base level and the YF, 32 km to the east (Fig. 4). Following the kinematic model, V and U decrease linearly from V_p = 6.0 mm/yr and U_p = 4.2 mm/yr at the western boundary to V_f = 4.1 mm/yr and U_f = 0 mm/yr immediately west of the YF. The domain to the east of the YF is horizontally fixed. To account for lithological variability along channels in west Lebanon, we simulate a dual-layer domain (see the Data Repository) with 800 m of resistant rock capping a softer, more erodible, layer at depth (Fig. 4).

Simulation results show that along with the upstream propagation of an incision wave, the western river channels are advected to the south and rotated counterclockwise. Despite small-scale reorganization in between neighboring basins of the western mountain flank and across the main water divide, the river basins act primarily as passive markers of the imposed horizontal crustal deformation (Movie DR1 in the Data Repository).

Distortion of drainage area of the western rivers during the simulation (Fig. 4; Movie DR1) results in preferential increase of χ values along southwest-flowing tributaries. This leads to a periodic variation of χ similar to the χ pattern found in western Mount Lebanon (compare Fig. 1 and Fig. 4).

DISCUSSION

The similarity of simulated and real drainage network geometry and spatial distribution of χ supports the hypothesis that western Lebanon rivers are reliable markers of horizontal distributed crustal deformation.

Figure 4. Results from landscape evolution simulation showing western flank of Mount Lebanon–like domain. Left: Drainage network after distributed and localized deformation following our kinematic model for 7.35 m.y., colored by χ value (see Equation 1). Note similarity of χ pattern between numerical rivers and western Lebanon rivers in Figure 1. Enlargements a–g illustrate χ differences across divides. Right: The same domain, colored by erodibility, showing exposure of older softer rocks (red) where total erosional exhumation is >800 m. More resistant rocks (blue) are preserved in highs and are advected across western base level. This results in lithological pattern similar to that of western Lebanon (Daëron, 2005). Simulated eastern side of numerical mountain range is not shown. Gray arrows represent imposed horizontal velocity field in western Mount Lebanon. R_d—width of band of deformation; DSFS—Dead Sea fault system.

The kinematic model described by Equations 2 and 3 defines a combined simple and pure shear deformation field. The simple shear rotates any marker not parallel to the YF and elongates markers that are sub-parallel to the YF. The pure shear results in shortening perpendicular to the YF, elongation in the vertical direction (uplift) (which is not part of the current two-dimensional analysis), and rotation of any marker that is neither parallel nor perpendicular to the YF.

This distributed deformation field can explain the observed χ pattern. Southwest-flowing tributaries of basins 2–6 flow in a direction of line elongation, while the width of their drainage area is in a shortening domain. As such, their catchments become longer and narrower during deformation, which results in an increase of χ (Equation 1). On the contrary, tributaries that flow to the west and northwest are shortened while their drainage area widens, leading to low χ values.

In the numerical model, we observe a competition between basin deformation and network reorganization. Capture events are observed along small tributaries of the western drainage network. These tend to shorten southwest-flowing tributaries and lengthen west- and northwest-flowing tributaries. This process is a response to the deformation of drainage basins: high-χ, southwest-flowing tributaries are captured by low-χ, west- and northwest-flowing tributaries that try to lengthen at the expense of the high-χ segments. High-χ tributaries are also captured by east-draining channels forming short-lived hook bends. The capacity for river capture depends on fluvial and hillslope geomorphic parameters, local incision rates, and local relief (Goren et al., 2014). In our model, geomorphic parameters are calibrated through a χ-z analysis (Perron and Royden, 2013) (see the Data Repository), and we observe that minor fluvial reorganization remains insufficient to amend the deformed drainage network. For this reason, χ differences across divides and rotated basins abound in the model.

The results of the kinematic analysis (Fig. 3) constrain the magnitude of the fault-parallel distributed deformation to the west of the YF to 1.6–2.2 mm/yr, which is 23%–31% of the relative fault-parallel plate velocity. The average slip rate along the YF since the late Miocene is found to be 3.8–4.4 mm/yr. This narrow range is within previous estimates of average slip rate along the YF for the Holocene and Quaternary (Gomez et al., 2007), and it indicates that average slip rate along the YF has remained constant since the late Miocene.

The distributed deformation field generates rotation about vertical and horizontal axes. To compare geomorphic and paleomagnetic measurements of rotation (McKenzie and Jackson, 1983), we calculated the expected rotation, θ, of a line marker when only simple shear is applied, i.e., when U = 0 (see the Data Repository). This is done because paleomagnetic measurements of declination are insensitive to the pure shear component (rotation about a horizontal axis). For the range of V_f = 3.8–4.4 mm/yr this scenario yields rotation of 20°–30°, consistent with the magnitude of counterclockwise rotation that has been inferred from paleomagnetic measurements, and in support of the view that the measured post-Cretaceous paleomagnetic rotation in west Lebanon relates to the post–late Miocene deformation in the DSFS (e.g., Ron, 1987; Henry et al., 2010).

Following Ron (1987), we suggest that distributed deformation in western Lebanon is accommodated by block rotation. The blocks are bounded by the YF, the Beirut-Tripoli thrust system, and smaller faults that stretch in between them (black lines in Fig. 1). This view is consistent with the right-lateral kinematics of the block-bounding faults (black lines in

Fig. 1), as confirmed by focal mechanism solutions (Salamon et al., 2003), by the parallelism between these faults and the orientation of the southwestern basins (pink lines in Fig. 1), and by significant micro-seismicity in the southern part of the deformation band (National Centre For Geophysical Research, 2015).

CONCLUSIONS

River orientation and pattern of drainage area disequilibrium contain retrievable information about modes and rates of horizontal deformation. Analysis and interpretation of river basin geometry in west Lebanon reveal that about one-quarter of the Arabia-Sinai plate motion parallel to the YF is distributed along a wide band to the west of the YF. We calculate an average slip rate on the YF since the late Miocene of 3.8–4.4 mm/yr. These rates are consistent with previous estimates obtained from Quaternary and Holocene markers, and thus suggest little variation of average slip rate since the late Miocene. We further demonstrate that rotation about a vertical axis as inferred from river orientation is consistent with paleomagnetic measurements. Modeling points toward a possible competition between basin deformation and drainage network reorganization. In the current setting, modeling shows minor reorganization that cannot compensate for the deformation and supports the view that rivers can serve as reliable markers of crustal horizontal distributed deformation in oblique convergence zones.

REFERENCES CITED

Ben-Avraham, Z., Garfunkel, Z., and Lazar, M., 2008, Geology and evolution of the southern Dead Sea fault with emphasis on subsurface structure: Annual Review of Earth and Planetary Sciences, v. 36, p. 357–387, doi:10.1146/annurev.earth.36.031207.124201.

Carton, H., et al., 2009, Seismic evidence for Neogene and active shortening offshore of Lebanon (Shalimar cruise): Journal of Geophysical Research, v. 114, B07407, doi:10.1029/2007JB005391.

Castelltort, S., Goren, L., Willett, S.D., Champagnac, J.D., Herman, F., and Braun, J., 2012, River drainage patterns in the New Zealand Alps primarily controlled by plate tectonic strain: Nature Geoscience, v. 5, p. 744–748, doi:10.1038/ngeo1582.

Daëron, M., 2005, Rôle, cinématique et comportement sismique à long terme de la faille de Yammoûneh, principale branche décrochante du coude transpressif libanais (faille du Levant) [Ph.D. thesis]: Paris, Institut de Physique du Globe de Paris, 179 p.

Daëron, M., Benedetti, L., Tapponnier, P., Sursock, A., and Finkel, R., 2004, Constraints on the post ~25-ka slip rate of the Yammoûneh fault (Lebanon) using in situ cosmogenic ^{36}Cl dating of offset limestone-clast fans: Earth and Planetary Science Letters, v. 227, p. 105–119, doi:10.1016/j.epsl.2004.07.014.

Elias, A., et al., 2007, Active thrusting offshore mount Lebanon: Source of the tsunamigenic A.D. 551 Beirut-Tripoli earthquake: Geology, v. 35, p. 755–758, doi:10.1130/G23631A.1.

Freund, R., Garfunkel, Z., Zak, I., Goldberg, M., Weissbro, T., and Derin, B., 1970, Shear along Dead Sea rift: Philosophical Transactions of the Royal Society A, v. 267, doi:10.1098/rsta.1970.0027.

Gomez, F., Khawlie, M., Tabet, C., Darkal, A., Khair, K., and Barazangi, M., 2006, Late Cenozoic uplift along the northern Dead Sea transform in Lebanon and Syria: Earth and Planetary Science Letters, v. 241, p. 913–931, doi:10.1016/j.epsl.2005.10.029.

Gomez, F., Nemer, T., Tabet, C., Khawlie, M., Meghraoui, M., and Barazangi, M., 2007, Strain partitioning of active transpression within the Lebanese restraining bend of the Dead Sea Fault (Lebanon and SW Syria), in Cunningham, W.D., and Mann, P., eds., Tectonics of Strike-Slip Restraining and Releasing Bends: Geological Society of London Special Publication 290, p. 285–303, doi:10.1144/290.10.

Goren, L., Willett, S.D., Herman, F., and Braun, J., 2014, Coupled numerical–analytical approach to landscape evolution modeling: Earth Surface Processes and Landforms, v. 39, p. 522–545, doi:10.1002/esp.3514.

Gregor, C.B., Mertzman, S., Nairn, A.E.M., and Negendan, J., 1974, Paleomagnetism and alpine tectonics of Eurasia: 5. The paleomagnetism of some Mesozoic and Cenozoic volcanic rocks from the Lebanon: Tectonophysics, v. 21, p. 375–395, doi:10.1016/0040-1951(74)90004-3.

Hallet, B., and Molnar, P., 2001, Distorted drainage basins as markers of crustal strain east of the Himalaya: Journal of Geophysical Research, v. 106, p. 13,697–13,709, doi:10.1029/2000JB900335.

Henry, B., Homberg, C., Mroueh, M., Hamdan, W., and Higazi, F., 2010, Rotations in Lebanon inferred from new palaeomagnetic data and implications for the evolution of the Dead Sea Transform system, in Homberg, C., and Bachmann, M., eds., Evolution of the Levant Margin and Western Arabia Platform since the Mesozoic: Geological Society of London Special Publication 341, p. 269–285, doi:10.1144/SP341.13.

Hovius, N., 1996, Regular spacing of drainage outlets from linear mountain belts: Basin Research, v. 8, p. 29–44, doi:10.1111/j.1365-2117.1996.tb00113.x.

Klinger, Y., Avouac, J.P., Dorbath, L., Abou Karaki, N., Bourles, D., and Reyss, J.L., 2000, Slip rate on the Dead Sea transform fault in northern Araba valley (Jordan): Geophysical Journal International, v. 142, p. 755–768, doi:10.1046/j.1365-246x.2000.00165.x.

Le Pichon, X., and Gaulier, J., 1988, The rotation of Arabia and the Levant fault system: Tectonophysics, v. 153, p. 271–294, doi:10.1016/0040-1951(88)90020-0.

McKenzie, D., and Jackson, J., 1983, The relationship between strain rates, crustal thickening, paleomagnetism, finite strain and fault movements within a deforming zone: Earth and Planetary Science Letters, v. 65, p. 182–202, doi:10.1016/0012-821X(83)90198-X.

National Centre For Geophysical Research, 2015, Seismicity of Lebanon 2006–2009: Beirut, Lebanon, National Council for Scientific Research, http://www.cnrs.edu.lb/download/pdf/all0609.jpg (accessed July 2015).

Perron, J.T., and Royden, L., 2013, An integral approach to bedrock river profile analysis: Earth Surface Processes and Landforms, v. 38, p. 570–576, doi:10.1002/esp.3302.

Quennell, A.M., 1984, The Western Arabia rift system, in Dixon, J.E., and Robertson, A.H.F., eds., The Geological Evolution of the Eastern Mediterranean: Geological Society of London Special Publication 17, p. 775–788, doi:10.1144/GSL.SP.1984.017.01.62.

Ramsey, L.A., Walker, R.T., and Jackson, J., 2007, Geomorphic constraints on the active tectonics of southern Taiwan: Geophysical Journal International, v. 170, p. 1357–1372, doi:10.1111/j.1365-246X.2007.03444.x.

Ron, H., 1987, Deformation along the Yammuneh, the restraining bend of the Dead Sea Transform: Paleomagnetic data and kinematic implications: Tectonics, v. 6, p. 653–666, doi:10.1029/TC006i005p00653.

Salamon, A., Hofstetter, A., Garfunkel, Z., and Ron, H., 2003, Seismotectonics of the Sinai subplate—The eastern Mediterranean region: Geophysical Journal International, v. 155, p. 149–173, doi:10.1046/j.1365-246X.2003.02017.x.

Sanderson, D.J., and Marchini, W.R.D., 1984, Transpression: Journal of Structural Geology, v. 6, p. 449–458, doi:10.1016/0191-8141(84)90058-0.

Shelef, E., and Hilley, G.E., 2014, Symmetry, randomness, and process in the structure of branched channel networks: Geophysical Research Letters, v. 41, p. 3485–3493, doi:10.1002/2014GL059816.

Teyssier, C., Tikoff, B., and Markley, M., 1995, Oblique plate motion and continental tectonics: Geology, v. 23, p. 447–450, doi:10.1130/0091-7613(1995)023<0447:OPMACT>2.3.CO;2.

Vallage, A., Devès, M.H., Klinger, Y., King, G.C.P., and Ruppert, N.A., 2014, Localized slip and distributed deformation in oblique settings: The example of the Denali fault system, Alaska: Geophysical Journal International, v. 197, p. 1284–1298, doi:10.1093/gji/ggu100.

Van Dongen, P., Van der Voo, R., and Raven, T., 1967, Paleomagnetism and the alpine tectonics of Eurasia: 3. Paleomagnetic research in the central Lebanon Mountains and in the Tartous area (Syria): Tectonophysics, v. 4, p. 35–53, doi:10.1016/0040-1951(67)90057-1.

Willett, S.D., McCoy, S.W., Perron, J.T., Goren, L., and Chen, C.Y., 2014, Dynamic reorganization of river basins: Science, v. 343, doi:10.1126/science.1248765.

Yang, R., Willett, S.D., and Goren, L., 2015, In situ low-relief landscape formation as a result of river network disruption: Nature, v. 520, p. 526–529, doi:10.1038/nature14354.